PNAS

Main Manuscript for

Light-Induced H_2 Generation in a Photosystem I-O_2-tolerant [FeFe] Hydrogenase Nanoconstruct

Tristen Rumbaugh[1], Michael J. Gorka[1]*, Carol S. Baker[2], John H. Golbeck[1,2]*, Alexey Silakov[1]*

[1]Department of Chemistry, The Pennsylvania State University, University Park, Pennsylvania, 16802, United States

[2]Department of Biochemistry and Molecular Biology, The Pennsylvania State University, University Park, Pennsylvania, 16802, United States

* Michael J. Gorka, **Email:** mjg382@psu.edu

* John H. Golbeck, **Email:** jhg5@psu.edu

* Alexey Silakov, **Email:** aus40@psu.edu

Author Contributions:

designed research: MG, JG, AS

performed research: TR, MG, CB

contributed new reagents or analytic tools: MG, CB, AS

analyzed data: TR, MG, AS

wrote the paper: TR, MG, CB, JG, AS

Competing Interest Statement: N/A

Classification: Biochemistry

Keywords: Hydrogenase, Photosystem I, dihydrogen generation, protein fusion, PsaE

This PDF file includes:

Main Text with 6 figures
Figures 1 to 6

Abstract

The fusion of hydrogenases and photosynthetic reaction centers has proven to be a promising strategy for the production of sustainable biofuels. Type I (iron-sulfur-containing) reaction centers, acting as photosensitizers, are capable of promoting electrons to a redox state that can be exploited by hydrogenases for the reduction of protons to dihydrogen (H_2). While both [FeFe] and [NiFe] hydrogenases have been used successfully, they tend to be limited due to either O_2 sensitivity, binding specificity, or H_2 production rates. In this study, we fuse a peripheral (stromal) subunit of Photosystem I (PS I), PsaE, to an O_2 tolerant [FeFe] hydrogenase from *Clostridium beijerinckii* using a flexible $[GGS]_4$ linker group (*Cb*HydA1-PsaE). We demonstrate that the *Cb*HydA1 chimera can be synthetically activated *in vitro* to show bidirectional activity and that it can be quantitatively bound to a PS I variant lacking the PsaE subunit. When illuminated in an anaerobic environment, the nanoconstruct generates H_2 at a rate of 84.9 ± 3.1 μmol H_2 mg_{chl}^{-1} hr^{-1}. Further, when prepared and illuminated in the presence of O_2, the nanoconstruct retains the ability to generate H_2, though at a diminished rate of 2.2 ± 0.5 μmol H_2 mg_{chl}^{-1} hr^{-1}. This demonstrates not only that PsaE is a promising scaffold for PS I-based nanoconstructs, but the use of an O_2-tolerant [FeFe] hydrogenase opens the possibility for an *in vivo* H_2 generating system that can function in the presence of O_2.

Significance Statement

Finding ways to generate dihydrogen (H_2) in an environmentally friendly way is an important challenge. The recent discovery of a robust, O_2-stable [FeFe] hydrogenase presents a unique opportunity for redirecting energy produced by Photosystem I to H_2 production in a phototrophic biological system that only requires sunlight and earth-abundant elements. Our study presents a strategy to couple such an [FeFe] hydrogenase to Photosystem I by fusing the former with a stomal subunit of Photosystem I (PsaE). Not only does the chimeric nanoconstruct generate reasonably high rates of H_2 when illuminated, but it also functions in the presence of O_2. By investigating catalytic properties and drawbacks of the nanoconstruct, this work sets the stage for engineering sustainable biofuel production *in vivo*.

Main Text

INTRODUCTION

Oxygenic photosynthesis drives a large fraction of life on earth by storing solar energy within chemical bonds through the act of CO_2 fixation and ATP formation. Central to this process are the two photosynthetic reaction centers (RCs), Photosystem I (PS I) and Photosystem II (PS II). These large pigment-protein complexes are found only in the thylakoid membranes of cyanobacteria, algae, and higher plants.

PS I is unique among Type I (iron-sulfur cluster) RCs, as its core is heterodimeric, containing a pseudo-symmetric arrangement of electron transfer cofactors (see Fig. 1A) (1, 2). The key electron transfer molecules bound to PsaA/PsaB core include six pseudo-symmetrical chlorophyll (Chl) *a* molecules consisting of a Chl dimer termed the primary donor P_{700} and the primary acceptors, A_A/A_B and A_{0A}/A_{0B} ("A" and "B" denote the subunit) (3). Following the absorption of a photon of light by a core or antenna Chl pigment, the excitation energy is transferred to P_{700}. The excited singlet state of P_{700} is followed by a donation of an electron to A_A/A_B or A_{0A}/A_{0B}, thereby initiating a charge-separated state. The electron is subsequently transferred through a phylloquinone (A_{1A} or A_{1B}), an [4Fe-4S] cluster, F_X, and finally to a pair of [4Fe-4S] clusters, F_A, and F_B, located in the PsaC subunit. The $P_{700}^{\bullet+}$ / $[F_A/F_B]^-$ charge-separated state has a sufficient lifetime to allow for a soluble [2Fe-2S] (plant-type) ferredoxin (Fd) to accept the electron from the $[F_A/F_B]^-$ clusters. The oxidized $P_{700}^{\bullet+}$ is subsequently reduced by plastocyanin or cytochrome (Cyt) c_6, thereby recovering the P_{700} ground state and resetting the system for a subsequent light-induced turnover.

An extensive chlorophyll antenna in PS I ensures a high cross-sectional area for photon capture with a quantum efficiency approaching unity, which means that virtually every photon is transferred to the core chlorophylls and converted into a charge-separated state. PS I (and PS II) are so efficient that during periods of high light intensity, the downstream processes of CO_2 fixation and ATP production cannot keep up with the reducing equivalents produced (4, 5). The efficiency of PS I presents an opportunity to direct the excess energy to alternative (engineered) pathways to power chemical transformations, such as the reduction of protons to produce dihydrogen (H_2).

Previous attempts to generate H_2 using PS I *in vitro* involved deposition of Au, Ru, Ir, Os, or Pt metals onto the stromal side of thylakoid membranes (6–10), implantation of Au and Pt nanoparticles (11–15), and the binding of cobaloxime and Ni-based catalysts (16). The use of metals has proven effective for the light-induced production of H_2. However, the need for expensive metals and the difficulty of generating these nanoconstructs *in vivo* present a significant drawback of this approach for utilization in commercially viable H_2 production. Engineering sustainable H_2-generating microorganisms by coupling PS I to an enzymatic H_2-producing system could be a rational alternative.

Hydrogenases are enzymes catalyzing the reversible oxidation of H_2. For PS I-based nanoconstructs, two superfamilies have been considered: [FeFe] hydrogenases and [NiFe] hydrogenases, named after the metal composition of their active site. [NiFe] hydrogenases are found in a wide variety of anaerobic and aerobic bacteria and archaea (17–19). [FeFe] hydrogenases comprise a functionally and structurally diverse superfamily typically found in obligate anaerobes (20). However, some green algae have been shown to express [FeFe] hydrogenases and produce H_2 under anaerobic conditions (21, 22). The ability of [FeFe] hydrogenases to produce H_2 at a higher rate than the energy throughput of PS I sparked widespread interest in this family of enzymes for biohydrogen production engineering efforts (23, 24).

Lubner et al. assembled a highly efficient nanoconstruct by directly coupling a [FeFe] hydrogenase from *Clostridium acetobutylicum* (*Ca*HydA1) to PS I using a molecular wire *in vitro* (23). This PS I-*Ca*HydA1 nanoconstruct achieved high rates of light-induced H_2 generation (up to 105 e^- PS I^{-1} s^{-1}, see table S1 in supporting information), outperforming electron transfer rates in natural photosynthesis by a factor of two. More recent work by Gorka et al. demonstrated an alternative strategy of utilizing A_{1A}/A_{1B}-based molecular wires to afford extraction of the electron from PS I (11, 12). One primary obstacle in utilizing wire-based coupling *in vivo* is the establishment of a molecular wire-S-[4Fe-4S] bond. It is thus unsurprising that despite the extraordinary success of these *in vitro* studies, no reports exist, to our knowledge, demonstrating the implementation of molecular-wire coupling strategies *in vivo*.

A more promising strategy for coupling PS I complex with a hydrogenase *in vivo* is by engineering a genetic fusion of the latter and one of the stromal subunits of PS I. Ihara et al. reported fusing a [NiFe] hydrogenase from the β-proteobacterium *Cupriavidus necator* H16 (formerly known as *Ralstonia eutropha* H16) to PsaE from *Thermosynechococcus elongatus* (25). More recently, Appel et al. demonstrated coupling of the native cyanobacterial [NiFe] hydrogenase from *Synechocystis sp*. PCC 6803 to PS I by fusion with PsaD (26). Unfortunately, these studies demonstrated low rates of light-driven H_2 evolution, most likely due to the bias of [NiFe] hydrogenases for H_2 uptake (27–29). Kanygin et al. generated chimera proteins formed between PsaC and [FeFe] hydrogenases HydA1 and HydA2 from *Chlamydomonas reinhardtii* (*Cr*) that complexed with PS I *in vivo* and generated H_2 in the light (30, 31). While the constructs performed exceptionally well in an anaerobic environment (see Table S1 in the supporting information), the authors reported a loss of hydrogenase activity under aerobic conditions, likely due to the O_2-induced degradation of the algal [FeFe] hydrogenases (30).

The sensitivity of [FeFe] hydrogenases to O_2 is well documented and, until recently, was thought to be a universal property of this class of enzymes that stems from the unique construction of the

active site (32–35). The active site of the [FeFe] hydrogenases (H-cluster) is composed of a [4Fe-4S] subcluster bound via a bridging cysteine thiolate to a labile [2Fe] subcluster. The Fe atoms of the subcluster are ligated by CO and CN^- and a bridging azadithiolate moiety (29, 36). In the presence of O_2, the H-cluster irreversibly degrades, likely involving a generation of reactive oxygen species at the open coordination site of the [2Fe] subcluster. Therefore, the presence of O_2 under photoautotrophy would inevitably result in an irreversible loss of hydrogenase activity (27, 32, 37).

It would seem as though the choice is between O_2 tolerance at the expense of H_2 generation or high rates of H_2 production in strictly anaerobic environments. However, the emergence of a subclass of O_2 tolerant [FeFe] hydrogenases (24, 32, 38) might allow PS I-[FeFe] hydrogenase nanoconstructs to be viable for light-driven H_2 generation in phototrophs. We have shown that [FeFe] hydrogenase from *Clostidium beijerinkii* (*Cb*HydA1) enters an O_2-protected state (termed H_{inact}) upon exposure to air. Notably, the reactivation requires a simple one-electron reduction of H_{inact} state. While the details of what confers O_2 stability are still under investigation, a structural study of *Cb*A5H, a close homolog of *Cb*HydA1, in the O_2-protected state suggests that Cys367 can act as a labile and protective cap, shielding the subcluster from O_2 (39). In support of this hypothesis, our recent Electron Paramagnetic Resonance (EPR) investigation provided evidence for enhanced protein mobility around the H-cluster in *Cb*HydA1 (40). Taken in concert with the recent work by the Happe group (41), these results suggest that protein flexibility may play a vital role in the ability of *Cb*HydA1 to access the O_2-protected H_{inact} state. Therefore, understanding whether a protein modification, e.g., fusion with PsaE, affects its O_2 tolerance and activity is paramount to the prospects for employing this enzyme or its homologs in phototrophic H_2 production.

In this work, we sought to investigate the feasibility of coupling *Cb*HydA1 to PS I complex from *Synechococcus sp*. PCC 7002 (hereafter *S*. 7002) by fusing *Cb*HydA1 with PsaE. We chose PsaE as the fusion counterpart due to the viability of PsaE-deletion variants of cyanobacteria (PS $I_{\Delta PsaE}$) (42). Aside from the [NiFe] hydrogenase-PsaE fusion, PsaE has also been used successfully for engineering PS I-based chimeric nanoconstructs for non-hydrogenase systems (43, 44).

We describe the design of the construct consisting of a modified *Cb*HydA1 connected to a 6X-His tagged PsaE protein via a flexible amino acid linker (4-times repeat of Gly-Gly-Ser), hereafter termed *Cb*HydA1-PsaE. We show that with the addition of the linker group and PsaE moiety, the hydrogenase retains bidirectional activity, albeit with some modification of activity. We also show that the presence of *Cb*HydA1 does not interfere with the binding of PsaE to PS $I_{\Delta PsaE}$. This PS I-*Cb*HydA1 nanoconstruct generates H_2 upon illumination in both anaerobic and aerobic conditions, opening the door to the creation of *in vivo* H_2-generating systems that utilize natural photosynthetic machinery.

RESULTS

Characterization of Cb*HydA1-PsaE Fusion Protein*

The *Cb*HydA1-PsaE fusion protein was designed by combining the amino acid code for *Cb*HydA1 followed by a $[GGS]_4$ linker, the code for wild-type PsaE from *S*. 7002, and a C-terminus His_6 tag to aid in purification (see Fig. 1 and Fig. S1). We truncated the *Cb*HydA1 domain at the N-terminus by 21 amino acids as this portion of the sequence is designated as a signaling sequence and thus may hinder the expression. To account for the potential differences in H-cluster assembly efficiency during synthetic maturation, we estimated the concentration of the fusion protein containing fully assembled H-cluster by incubating samples under a carbon monoxide atmosphere and subsequently quantifying the amount of H_{ox}-CO state by continuous wave (CW) EPR (see materials and methods and Fig. S9).

Intriguingly, the hydrogenase activity analysis indicates that the enzymatic activity of the *Cb*HydA1-PsaE fusion protein obtained using this methodology is about 3-fold lower than that of *Cb*HydA1$_{WT}$ (see Fig. 2). We estimated the rate of H_2 uptake to be 524 ± 156 µmol H_2 $mg_{prot}^{-1}min^{-1}$ and 173 ± 33 µmol H_2 $mg_{prot}^{-1}min^{-1}$ for holo-*Cb*HydA1$_{WT}$ (Fig. S3) and holo-C*b*HydA1-PsaE (Fig. S4), respectively. H_2 evolution assays provided a specific activity of 1087 ± 92 µmol H_2 $mg_{prot}^{-1}min^{-1}$ and 534 ± 70 µmol H_2 $mg_{prot}^{-1}min^{-1}$ for holo-*Cb*HydA1$_{WT}$ (Fig. S3) and holo-*Cb*HydA1-PsaE (Fig. S4) fusion proteins, respectively.

To investigate whether the difference in the activity of the wild-type and fusion proteins is due to a difference in the electronic structure of the H-cluster, we performed a series of Fourier-transform infrared (FTIR) spectroscopy measurements, focusing on CO and CN^- stretching bands of the H-cluster (38). The *Cb*HydA1-PsaE fusion protein obtained immediately after activation with the synthetic $[2Fe]_H$ precursor (labeled "as prepared") exhibited a mixture of IR signals characteristic of the H_{ox}, the $H_{red}H^+$, and H_{ox}-CO states with the CO/CN^- band positions matching well those reported in the literature for *Cb*HydA1$_{WT}$ (see Figs. 3A, S5) (38). Upon exposure to air for 20 min, FTIR spectra of the fusion protein (Fig. 3B) exhibit a complete conversion of the H-cluster to the inactive state (H_{inact}) identical to that of *Cb*HydA1$_{WT}$ (38). We were able to reactivate the H-cluster by incubation with 1 atm H_2 after exposure to air (Fig. 3C). We also observed that the *Cb*HydA1-PsaE fusion protein can be inhibited with CO, exhibiting a typical IR spectrum of the H_{ox}-CO state (Fig. 3C). Finally, as for *Cb*HydA1$_{WT}$, the H_{ox}-CO state of *Cb*HydA1-PsaE fully converts into the H_{inact} state (Fig. 3E) upon consequent exposure to air. Overall, this set of experiments demonstrates that the fusion of *Cb*HydA1 with PsaE does not noticeably affect the electronic structure of the H-cluster and its interaction with diatomic gases (H_2, O_2, and CO). Furthermore, it appears that *Cb*HydA1-PsaE retains the ability to convert into the H_{inact} state under aerobic conditions, either from the active or the CO-inhibited states.

The catalytic ability of the *Cb*HydA1-PsaE fusion protein was further analyzed using protein film voltammetry (PFV), in which protein is adsorbed on a rotating disk electrode. In cyclic voltammetry (CV) experiments using a protein-coated working electrode, a positive current indicates H_2 uptake, while a negative current signifies H^+ reduction (45–47). In the case of *Cb*HydA1$_{WT}$, a drop of current at higher potentials is expected due to the enzyme's conversion to the H_{inact} state (38). We evaluated the *Cb*HydA1-PsaE fusion protein at various pH values to assess potential differences in the pH dependence of the catalysis from the wild-type counterpart (see Fig. 4). Overall, the pH dependence of CV traces are remarkably similar to the typical response observed for *Cb*HydA1$_{WT}$. Importantly, the fusion protein inactivates with a forward sweep to higher potentials and reactivates with a backward sweep. Quite intriguingly, a comparison between *Cb*HydA1$_{WT}$ and *Cb*HydA1-PsaE shows a shift of the reactivation wave to lower potentials for the latter. This discrepancy is more prominent at higher pH values, with about 95 mV downshift of the mid-point of reactivation (E_{switch} (48)), but it is still noticeable at lower pH values (60-74 mV difference). A lower apparent mid-point potential for the reactivation of *Cb*HydA1-PsaE suggests a higher propensity of *Cb*HydA1-PsaE to remain in the H_{inact} state relative to *Cb*HydA1$_{WT}$ (41, 49). This increased tendency to inactivate may contribute to the lower activity of the fusion protein in the *in vitro* activity assays described above, although further investigation is needed to confirm this point.

Binding of C*b*HydA1-PsaE Fusion Protein to PS I$_{\Delta PsaE}$

To assess the ability of the *Cb*HydA1-PsaE fusion protein to bind to the ΔPsaE variant of PS I (PS I$_{\Delta PsaE}$), and to assess the efficacy of forward electron transfer in this orthogonal pathway, we performed time-resolved optical experiments. The time-resolved absorption at 830 nm reports on the reduction of $P_{700}^{\bullet+}$ after a 7-ns, single-turnover actinic laser flash at 532 nm. $P_{700}^{\bullet+}$ reduction can occur from either a reduced acceptor in the electron transfer chain (termed charge recombination), or an exogenous electron donor (ascorbate, DCPIP, Cyt c_6, etc.). Charge recombination kinetics from every cofactor in the acceptor chain have been well characterized for

PS I_{WT} and numerous PS I variants (50–53). Deviations from those values serve as a reliable diagnostic tool for understanding changes in cofactor energetics within the complex (30, 51).

The kinetics of $P_{700}^{\bullet+}$ decay after an actinic flash in the presence of ascorbate as an electron donor are shown in Fig. 5, along with the respective component analysis. The complete set of $P_{700}^{\bullet+}$ decay is shown in the supporting information (see Fig. S6). To provide a model-free assessment of the decay traces, we employed inverse Laplace transformation analysis by CONTIN (see materials and methods) (54). As expected, PS I_{WT} displays a largely monophasic decay with a lifetime of ~100 ms, closely matching the previously measured recombination between $[F_A/F_B]^-$ and $P_{700}^{\bullet+}$ (see Fig. S6). The PS $I_{\Delta PsaE}$ variant (Fig. 5A) appears to display a largely monophasic $P_{700}^{\bullet+}$ reduction but with a noticeably slower decay with a dominant lifetime of 381 ms (58%). This change is consistent with previous reports in an *in vivo* PsaE deletion mutant of *S*. 7002 (55).

Although the origin of the alterations to $P_{700}^{\bullet+}$ decay kinetics imposed by the absence of PsaE is not understood (see discussion), the change is a reliable reporter for the binding of PsaE to PS I. We used this finding to investigate the binding of the *Cb*HydA1-PsaE fusion protein to PS $I_{\Delta PsaE}$ *in vitro*. First, we performed binding experiments on the apo-form of the fusion protein lacking the H-cluster (apo-*Cb*HydA1-PsaE). Upon anaerobic addition of apo-*Cb*HydA1-PsaE fusion protein to PS $I_{\Delta PsaE}$ in a 3-fold excess, the $P_{700}^{\bullet+}$ reduction kinetics remain mostly monophasic and closely resemble those of PS I_{WT} (see Fig. 5B and Fig. S6), with lifetimes of 122 ms (~54%) and a smaller contribution from a faster decay kinetic with lifetime of 25 ms (~20%). The absence of the 381 ms reduction phase suggests a near-quantitative binding of the fusion protein to PS I.

Next, we performed similar experiments on the active fusion protein, expecting a significant elongation of the $P_{700}^{\bullet+}$ lifetime due to the loss of e^- to H_2 production by the hydrogenase domain. In this case, regeneration of the P_{700} ground state is only possible via reduction by an exogenous electron donor. Slow donors, such as ascorbate, reduce $P_{700}^{\bullet+}$ in a matter of several seconds. However, the holo-*Cb*HydA1-PsaE:PS $I_{\Delta PsaE}$ complex (Fig. 5B,D) kept under a 3% H_2 + 97% N_2 atmosphere exhibited a somewhat faster $P_{700}^{\bullet+}$ decay than that of PS I_{WT}. As shown by iLT, the kinetic decay is heterogeneous, with a dominant process consisting of two phases at 43 ms and 96 ms (together contributing ~68% to the total decay) and a smaller contribution from a slower bi-phasic decay (~23%). This is a stark departure from the apo-*Cb*HydA1-PsaE:PS $I_{\Delta PsaE}$ sample, suggesting an alteration to the charge recombination pathways in the presence of the active hydrogenase domain. Most notably, the CONTIN analysis of this dataset reveals the complete absence of a >1s charge recombination. We hypothesized that holo-*Cb*HydA1-PsaE acts as a reductant of the FeS clusters in PsaC in the presence of H_2 effectively shutting down forward electron transfer. Consequently, we repeated the same experiments under a pure He atmosphere, which should bias the evidently bidirectional hydrogenase domain (see PFV experiments above) towards H_2 evolution. Under this condition, the PS I-*Cb*HydA1 complexes (Fig. 5B,D, Fig. S6) display a noticeably different multiphasic decay of $P_{700}^{\bullet+}$. The kinetics with lifetimes of 28.5 ms (17.5%) and 128 ms (40%) are highly similar to that of apo-*Cb*HydA1-PsaE:PS $I_{\Delta PsaE}$. In addition, there is another substantial phase at >3 sec (28.0%). This long-lived phase indicates $P_{700}^{\bullet+}$ reduction via ascorbate, suggesting electron loss due to forward electron transfer from PS I to the [FeFe] hydrogenase domain. Note that we have estimated a 32% yield of the fully assembled H-cluster (see materials and methods). This fraction of active fusion protein matches well with the 28% contribution of the long-lived phase, suggesting a high efficacy of the forward electron transfer to the H-cluster in the holo-*Cb*HydA1-PsaE:PS $I_{\Delta PsaE}$ nanoconstruct. However, as we will discuss below, such extrapolation must be done with care.

Light-Induced H_2 Generation by the Nanoconstruct

We next sought to quantify the amount of H_2 generated by the PS I-*Cb*HydA1 complex by conducting gas chromatography (GC) analysis of the sample's headspace in a capped vial under illumination with a 100 W xenon arc lamp. Before the analysis, the headspace of each sample vial

was purged in the dark with ultra-pure He (UHP He) for 20 minutes to remove residual H_2 from the anaerobic chamber atmosphere. The rate obtained for the anaerobically prepared PS I-*Cb*HydA1 nanoconstruct (Figs. 6A, S8A) is 84.9 ± 3.1 μmol H_2 mg_{chl}^{-1} hr^{-1} (4.05 e^- PS I^{-1} sec^{-1}). We detected small amounts (0.44–0.74 μmol H_2 mg_{chl}^{-1} hr^{-1}) of H_2 in control experiments, including the blank buffer sample. The detection of H_2 in controls is likely due to outgassing residual dissolved H_2 in the sample solution (prepared under 3% H_2 / 97% N_2 atmosphere) after purging with UHP He. The sample lacking PS $I_{\Delta PsaE}$ is the exception, showing an increased rate equivalent to 1.8 ± 0.4 μmol H_2 mg_{chl}^{-1} hr^{-1} under identical sample conditions, indicating some residual hydrogenase activity likely due to the presence of a large excess of ascorbate in the sample.

To assay aerobic H_2 generation by the designed nanoconstruct, we repeated the above experiments, but allowing samples to incubate on air for at least2 hours prior to capping the GC vial to accumulate H_2. The rate of light-induced H_2 production for these samples was noticeably lower than the anaerobically prepared samples, 2.2 ± 0.5 μmol H_2 mg_{chl}^{-1} hr^{-1} (0.10 e^- PS I^{-1} sec^{-1}), (see Figs. 6B, S8B). As expected, we detected no H_2 generated in most control experiments since the sample vials were kept in the air outside an anaerobic chamber with no possibility of H_2 leaching into the sample space. However, the PS $I_{\Delta PsaE}$ sample ("no fusion" in Fig. 6) did show small amounts of H_2 produced when prepared at 12-fold higher concentrations than the anaerobically prepared samples. Under these conditions, the rate of H_2 production was estimated to correspond to 0.053 ± 0.005 μmol H_2 mg_{chl}^{-1} hr^{-1}. It should be noted that minor H_2 production by PS $I_{\Delta PsaE}$ alone parallels observations by Ihara et al., who observed small amounts of H_2 produced from a Cyt c_3/PS I complex (56). Also, in the high-concentration sample of *Cb*HydA1-PsaE fusion protein (no PS $I_{\Delta PsaE}$), we were able to observe detectable H_2 production that would correspond to 0.0036 ± 0.0001 μmol H_2 mg_{chl}^{-1} hr^{-1} (calculated with an equimolar fusion:PS I ratio) indicating that a small fraction of hydrogenases remains active, even under aerobic conditions in the presence of ascorbate.

DISCUSSION

Fusion of PsaE to Cb*HydA1 changes its catalytic activity.*

Our experiments indicate a measurable impact of the fusion of PsaE on the activity of *Cb*HydA1, as evident from two- to three-fold lower H_2 oxidation and proton reduction rates than that of a wild-type protein. In protein film voltammetry experiments, we observed an increased propensity of the *Cb*HydA1 for inactivation in the PsaE-fusion variant compared to the wild-type enzyme. The shift of the reactivation CV wave to a lower potential in the *Cb*HydA1-PsaE fusion protein can be a consequence of either a lower mid-point reduction potential of the H_{inact} state or faster kinetics of inactivation (39, 40).Recently, using EPR, we demonstrated the existence of two structural isoforms of *Cb*HydA1. We proposed that the unique-to-*Cb*HydA1 isoform 1 (EPR signals $H_{ox}(1)$ and H_{ox}-CO(1)) is the inactivation-preceding form that relates to the aberrant position of the Cys367 facilitated by a rearrangement of the respective flexible loop (39, 40). The dominance of the isoform 1 in EPR measurements of CO-inhibited *Cb*HydA1-PsaE variant (see Fig. S7) is in line with the observed downshift of the reactivation wave in PFV. Therefore, we consider it likely that adding PsaE to *Cb*HydA1 affects the mobility of the core protein structure around the H-cluster, resulting in an increased propensity for inactivation in the fusion protein and, thus, lower activity. Furthermore, isoform 1 may naturally be less active since it proposedly relates to an off-H^+-pathway arrangement of Cys367 (40).

We also cannot exclude the possibility that the fusion of PsaE to *Cb*HydA1 could affect the electronic structure of the two accessory [4Fe-4S] clusters (F-clusters) present in the enzyme. Indeed, there is a slight but noticeable shift in the ratio between H_2 evolution and H_2 uptake towards the former in the fusion protein. Also, as-prepared WT and fusion enzymes obtained under identical conditions show somewhat different ratios of H_{ox} and $H_{red}H^+$ states in IR (see Fig S5), possibly due to a somewhat different catalytic bias causing a shift of equilibrium between the two states.

However, as both catalytic rates are lower in the fusion protein, further investigation into the redox potentials of the F-clusters is needed to understand this effect fully. Such experiments are underway in our laboratory.

Electron transfer in the modified PS I complexes.

Our study of the $P_{700}^{\bullet+}$ reduction kinetics after an actinic laser pulse provided invaluable insights into the electron transfer mechanisms with the modified PS I complexes. First, the experiments confirmed the early report by Yu, et al. (55) that the absence of PsaE elongates the lifetime of $P_{700}^{\bullet+}$-$[F_A/F_B]^-$ charge-separated state. Charge recombination rates are inextricably tied to the redox potential of the bound cofactors, the reorganization energies associated with the site, and the distance between the cofactors. Hence, our working hypothesis is that the lack of a PsaE subunit affects the mobility of the PsaC and PsaD subunits, ultimately resulting in a shift in the redox potential of either F_A and F_B or their distance from F_x and thus causing a change in the lifetime of the charge-separated state. While understanding this effect is outside the scope of this work, it is an important line of research to address in the future, as the structural modifications imposed on PsaE by the fusion with *Cb*HydA1 may pose additional effects on the electron transfer pathways within the PS I complex.

Incubation of PS $I_{\Delta PsaE}$ with apo- and holo-*Cb*HydA1-PsaE results in a shift to PS I_{WT}-like $P_{700}^{\bullet+}$-$[F_A/F_B]^-$ recombination lifetimes, thus indicating a near-quantitative formation of the PS $I_{\Delta PsaE}$:*Cb*HydA1-PsaE complex. It is somewhat surprising that when we incubate PS $I_{\Delta PsaE}$ with the apo-form of the fusion protein (F-clusters present, but no active site), there is very little of the long-lived phase, implying almost no electron transfer from PS I to the hydrogenase. However, it is important to note that the resulting data is averaged over 512 traces. Without an electron acceptor such as the active center (H-cluster), the F-clusters will likely remain reduced after the first couple of flashes for the duration of the experiment, assuming a high quantum yield of electron transfer. As a result, forward electron transfer from F_A/F_B to the hydrogenase domain will be effectively blocked. The time-resolved optical experiments on PS $I_{\Delta PsaE}$:holo-*Cb*HydA1-PsaE nanoconstruct in the presence of H_2 demonstrate that the electron transfer from $[F_A/F_B]^-$ to the F-cluster is not entirely unidirectional. Were that the case, H_2 oxidation by the H-cluster would result in a reduction of the F-cluster but not the $[F_A/F_B]$ pair, and hence, we would expect kinetic traces to be similar to that of PS $I_{\Delta PsaE}$:apo-*Cb*HydA1-PsaE. To the contrary, our time-resolved experiments showed that under a 3% H_2 atmosphere, the charge recombination is substantially more complex. CONTIN analysis shows a complex multiphasic kinetic profile with the dominant decay phase being faster than that observed in the PS $I_{\Delta PsaE}$:apo-*Cb*HydA1-PsaE nanoconstruct. Therefore, the data indicate that the H_2-uptake by the hydrogenase domain not only saturates the F-cluster, but also partially reduces the $[F_A/F_B]$ couple. This "backfire" effect could inhibit forward electron transfer within PS I, potentially accelerating charge recombination. In line with this suggestion, the removal of H_2 from the headspace resulted in a substantial elongation of the charge recombination lifetime. In this case, two primary decay phases are the PS I_{WT}-like lifetime of ~100 ms and a long-lived charge-separated state >3 sec. The long-lived phase, whereby $P_{700}^{\bullet+}$ is reduced by ascorbate, increases in amplitude from ~4% of the total signal to ~30%. This increase provides compelling evidence for the forward electron transfer from PS I to hydrogenase with the consequent loss of the electron to proton reduction. The remaining 100 ms phase is likely wherein the fusion protein is bound, but forward electron transfer is not occurring in PS I. We note that in our spin-quantification experiments, only a third of *Cb*HydA1-PsaE fusion proteins contain a fully assembled H-cluster (see supporting information). This alone could be sufficient to explain why forward electron transfer is only 31% efficient. However, whether there is a preference for binding holo-*Cb*HydA1-PsaE rather than apo-*Cb*HydA1-PsaE to PS $I_{\Delta PsaE}$ is not known, as discussed below.

Comparison with other nanoconstructs

The H_2 production rate we observe for our nanoconstruct is 84.9 ± 3.1 µmol H_2 mg_{chl}^{-1} hr^{-1} is similar to other PS I-nanoconstructs tested under roughly comparable conditions (see Table S1) (11–15, 23, 25, 56–63). Due to sub-par H-cluster incorporation rate of ~31% for the *Cb*HydA1-PsaE fusion protein, the maximum theoretical rate could be upwards of ~250 µmol H_2 mg_{chl}^{-1} hr^{-1} or ~12 e^- $(PS\ I)^{-1}s^{-1}$. However, we refrain from using such an extrapolation as many factors can contribute to the overall quantum yield. While data suggests a near-quantitative binding of a fusion protein to PS $I_{\Delta PsaE}$, it is possible that there is a binding preference of apo- vs holo-proteins, or steric limitations on the trimer affecting the number of *Cb*HydA1 domains able to interact with PsaC while bound. Also the ratio between forward electron transfer and charge recombination rates may play a role, as well as the "backfire" effect discussed above.

When discussing related PS I-based nanoconstructs, perhaps the most appropriate comparison would be that with the PsaC-fusion variants of [FeFe] hydrogenases 1 and 2 from *Chlamydomonas reinhardtii* (30, 31). The overall electron throughput of these systems, as determined experimentally, appears to be 8–70 times higher than that observed in our case (see Table S1). However, these measurements were carried out under *in vivo* conditions where reduction of $P_{700}^{\bullet+}$ occurs via natural and efficient electron transport, while we utilized a soluble Cyt c_6 as an electron donor *in vitro*. Hence, the H_2 production rate is likely rate-limited in the latter by the recycling of P_{700} rather than by the performance of the active chimeric nanoconstructs. Note that crosslinking Cyt c_6 to PS I resulted in a nearly 7-fold increase in H_2 production rate in the PS I--wire-*Ca*HydA1 nanoconstructs reported by the Golbeck group under comparable conditions, with a maximum 70-fold increase achieved by lowering pH (up to 2200 µmol H_2/mg_{Chl}/hr, see Table S1) (23). It would thus be interesting to perform similar Cyt c_6 crosslinking experiments for our nanoconstructs to estimate the maximum possible H_2 production rate for the *Cb*HydA1-PsaE:PS $I_{\Delta PsaE}$ nanoconstruct.

The nanoconstruct can generate H_2 under aerobic conditions.

Demonstrating detectable H_2 production by the nanoconstruct under aerobic conditions is highly encouraging. It is important to note that there are several avenues by which O_2 can interrupt energy and electron transfer both within PS I and between PS I and the hydrogenase. Within PS I complex, O_2 can react with Chl triplet states during light harvesting (64). O_2 can also accept low-potential electrons from $[F_A/F_B]^-$ cluster pair and even from the A_1 phylloquinones (65–67). A gradual reduction in O_2 concentration in the headspace (Figure S8B) supports this notion. Therefore, electron transfer from $[F_A/F_B]^-$ to *Cb*HydA1 is in competition not only with charge recombination but also with the reduction of molecular oxygen. For *Cb*HydA1, O_2 will also functionally inactivate the active site, requiring reducing equivalents from PS I for periodic reactivation. Given this combination of factors, it is not surprising that the rates of H_2 production by the *Cb*HydA1-PsaE:PS I nanoconstruct are lower than for anaerobically prepared samples. It may be possible to improve the efficiency of the forward electron transfer by varying the length and rigidity of the linker group to increase both protein activation, specific activity, and electron transfer from PS I. Further investigation into the interaction of O_2 with the parts of the nanoconstructs will be required to parse out the contributing factors and devise a mitigation strategy. Nonetheless, even with reduced rates in the presence of O_2, the *Cb*HydA1-PsaE:PS I nanoconstruct shows promise for an *in vivo* system that functions in the presence of constantly changing levels of O_2.

In summary, we have successfully generated a unique chimeric protein nanoconstruct through the fusion of a 7.6 kDa stromal subunit of PS I (PsaE) from the cyanobacterium *Synechococcus sp*. PCC 7002 onto the C-terminus of an oxygen-tolerant [FeFe] hydrogenase from *Clostridium beijerinckii* (*Cb*HydA1) via a flexible $[GGS]_4$ linker group. We show that *Cb*HydA1 can be synthetically activated *in vitro* and retain native-like bidirectional hydrogenase activity. Our transient absorption studies demonstrate that the PsaE substituent provides a mode for selective and nearly quantitative binding of the fusion protein to available PS $I_{\Delta PsaE}$-cores. We were able to detect light-induced H_2 evolution even in an aerobic environment. Our findings provide confidence in PsaE as a viable scaffold for the binding of exogenous proteins to PS I cores. The detailed investigation of the H_2-producing chimeric nanoconstruct presented here establishes an important basis for

future engineering *in vivo* H_2-generating systems that can function within O_2-evolving photosynthetic pathways.

MATERIALS AND METHODS

Preparation of Protein Samples. *Cb*HydA1-PsaE and *Cb*HydA1$_{WT}$ were expressed and purified similarly to methods found in the literature (38). In short, the protein was expressed in *Escherichia coli* BL21 (DE3) Δ*iscR* strain (The Pennsylvania State University, Golbeck lab) (68). Luria-Bertani (LB) growth medium (3L) was supplemented with 100 mM MOPS pH 7.4, 2 mM ferric ammonium citrate, 2 mM L-cysteine, and 100 µg/mL ampicillin. Cultures were first grown aerobically at 37°C to an O.D.$_{600}$ of 0.6 ± 0.2. Then, placed on ice, further supplemented with 0.5% glucose and 25 mM sodium fumarate, and brought inside an anaerobic chamber. Cultures were induced anaerobically with the addition of 1.5 mM IPTG and allowed to express for 20 hours at 20°C. The cells were lysed via anaerobic sonication for 1 hour with continuous stirring. After centrifugation, the *Cb*HydA1-PsaE fusion protein was purified using a Co-NTA affinity chromatography (Fig. S2). The purified protein was buffer-exchanged using a PD-10 column into a buffer containing 100 mM HEPES, pH 7.5, 5 mM dithiothreitol, 300 mM KCl. Protein yields averaged ~3.5 mg per L of cell growth. Reconstitution of the iron-sulfur clusters was performed through a slow addition of 15-fold excess $FeCl_3$•$6H_2O$ and Na_2S•$9H_2O$, consecutively, over the course of 30 minutes and 60 minutes, respectively. Synthetic maturation using a $[2Fe]_H$ synthon $Fe_2[\mu\text{-}S_2C_2H_4NH](CO)_4(CN)_2$ was performed according to previously published procedures (38). PS I_{WT} and the PS $I_{\Delta PsaE}$ variant were isolated from variants of *Synechococcus sp*. PCC 7002 using previously reported methods (Fig. S10) (55, 69), with some modifications as described in detail in the supporting information.

Quantification of H-cluster Incorporation. To account for a potentially inefficient H-cluster assembly during synthetic maturation, we estimated concentrations of the fully assembled H-cluster by incubating samples with CO and subsequently quantifying the amount of the H_{ox}-CO state by continuous wave (CW) electron paramagnetic resonance (EPR) spectroscopy. The fusion protein was incubated under CO gas for 30 minutes before analysis via CW EPR (Fig. S7). We used FTIR to confirm the complete conversion of the H-cluster to the H_{ox}-CO state. The power dependence of the double integral of the H_{ox}-CO EPR signals was compared to that of the standard (321 µM MbN_3, Fig. S9), from which the concentration of the H-cluster in the sample was extracted. This concentration was then compared against the concentration of protein determined by the Bradford assay to calculate the percent of H-cluster incorporation. For the samples used in the experiments presented here, H-cluster synthesis efficiency was estimated to be 63% and 31% for *Cb*HydA1$_{WT}$ and C*b*HydA1-PsaE, respectively. These correction factors were used in all reported hydrogenase activity values.

EPR and FTIR spectroscopy. EPR spectra reported were obtained using Magnettech MS5000 X-band spectrometer augmented with a liquid He flow cryostat (Oxford Instruments ESR900). For the measurements, 250 µL of samples were placed in a 4mm OD clear fused quartz tube.

FTIR measurements were made on a Nicolet is50 FTIR (Thermos Scientific) spectrometer equipped with an LN_2-cooled MCT-A detector with a 3.6 µm long-pass filter (Edmund Optics). Experiments were conducted in a home-built cell consisting of two 32 mm OD, 2 mm thick CaF_2 windows, with a 40 µm PTFE spacer. All samples were prepared and measured at room temperature. Data sets were collected with 2000 scans with a resolution of 2 cm^{-1}. All EPR and FTIR spectra were processed in MATLAB using home-build software (Kazan viewer, https://github.com/AlexeySilakov/KazanViewer/).

Protein Film Voltammetry. Protein film voltammetry (PFV) measurements were made in an anaerobic chamber (Coy Laboratory Products, Inc.) with a WaveNow potentiostat (Pine Research), with a variable-speed rotator (Pine Research). Measurements were performed using a home-built

rotating disc electrode using a 5 mm OD edge-plane pyrolytic graphite PG-HT encased in a 12 mm OD PEEK cylinder. The surface of the electrode was first polished using 2000 grit sandpaper and then sonicated in 50% ethanol. The reference electrode used was a 3 M NaCl Ag/AgCl electrode (BASi MF-2052). The counter electrode was a Pt wire wound into a spiral (Sigma Aldrich, 0.25 mm OD). Calibration of the reference electrode was performed using a methyl viologen solution, $E_0(MV^{2+}/MV^{\bullet+})$ = -445 mV vs NHE.

Time-Resolved Optical Spectroscopy. A detailed description of the home-built set-up is provided elsewhere (52). An actinic laser flash at 532 nm with a pulse width of 7 ns (full-width half-maximum) generates a single turnover event in PS I. Changes in absorbance were monitored via an 830 nm laser diode (CrystaLaser, model number DL830-100-O) that is split into measuring and reference beams. The difference signal was amplified with a 200 MHz bandwidth differential amplifier (Thor Labs PDB460A), which was subsequently processed using a 1 GHz bandwidth, 8-bit, 2 GS/s, PCI card (National Instruments NI-5154) controlled by a home-built software. Data analysis was performed using home-built software in Python. Regularized inverse Laplace transformations of kinetic decay traces were performed using CONTIN software (54). Regularization order (mode) was set to NORDER=2, and the regularization parameter was set to ALPST=2E-5; the program was restricted to finding non-negative solutions (NONNEG=1) as no subsequent oxidation of P_{700} is expected after the initial generation of the charge-separated state under conditions used. All samples contained a Chl concentration of 100 µg/mL, corresponding to a concentration of 1.16 µM PS I, Tris-HCl (pH 8.0), 500 µM sodium ascorbate, and 0.05% (w/v) β-DDM). More details on sample preparation can be found in the supplemental information.

Light-Induced H_2 generation. *Cb*HydA1-PsaE:PS $I_{\Delta PsaE}$ nanoconstructs were generated anaerobically through a 30-minute incubation of PS $I_{\Delta PsaE}$ with the *Cb*HydA1-PsaE fusion protein in a ratio of 1 : 3, PS I : *Cb*HydA1-PsaE. Following incubation, the solution was washed 5 times with 50 mM Tris pH 8.0, 50 mM NaCl, and 0.05% β-DDM through a 100 kDa Centricon centrifugal filter (Amicon Ultra, 0.5 mL). H_2 production rates were determined in accordance with previously published methods (23, 57, 58). 500 µL of the assembled PS I–*Cb*HydA1 nanoconstruct solution was placed into a 8 mL glass vial, capped with a gray-butyl septa, and kept in the dark. A sacrificial electron donor (100 mM ascorbate) and 20 µM Cyt c_6 (Figure S11) were added for reduction of P_{700}^+. For anaerobic experiments, the vial was purged with ultra-pure He for 20 minutes to remove residual anaerobic chamber dihydrogen. Samples were measured immediately before and periodically during illumination. For aerobic experiments, samples were equilibrated on air before capping for at least two hours and the headspace was not displaced. The headspace was analyzed with a Shimadzu GC-2010 Plus gas chromatograph equipped with a RT-Msieve 5A column (Restek) and a barrier ionization detector (BID 2010 Plus), using ultra-pure He as the carrier gas with a linear velocity of 42.5 cm/s. The injection temperature was 150°C, the column temperature was 35°C, and BID temperature was 280°C.

DATA, MATERIALS, AND SOFTWARE AVAILABILITY

All study data are included in the article and/or SI Appendix.

ACKNOWLEDGMENTS

We would like to acknowledge Dr. Patrick Corrigan for supplying the synthon used for *in vitro* protein maturation. This material is based upon work supported by the U.S. Department of Energy, Office of Science, Office of Basic Energy Sciences program under Award Number DE-SC0018087 (to A.S, J.H.G., M.G.) and by the National Science Foundation under Grant No. CHE-1943748 (to A.S).

REFERENCES

1. P. Jordan, *et al.*, Three-dimensional structure of cyanobacterial photosystem I at 2.5 Å resolution. *Nature* **411**, 909–917 (2001).

2. P. Fromme, P. Jordan, N. Krauß, Structure of photosystem I. *Biochimica et Biophysica Acta (BBA) - Bioenergetics* **1507**, 5–31 (2001).

3. M. Gorka, *et al.*, Shedding Light on Primary Donors in Photosynthetic Reaction Centers. *Front Microbiol* **12** (2021).

4. R. R. Sonani, *et al.*, Site, trigger, quenching mechanism and recovery of non-photochemical quenching in cyanobacteria: recent updates. *Photosynth Res* **137**, 171–180 (2018).

5. R. Bassi, L. Dall'Osto, Dissipation of Light Energy Absorbed in Excess: The Molecular Mechanisms. *Annu Rev Plant Biol* **72**, 47–76 (2021).

6. J. F. Millsaps, B. D. Bruce, J. W. Lee, E. Greenbaum, Nanoscale Photosynthesis: Photocatalytic Production of Hydrogen by Platinized Photosystem I Reaction Centers. *Photochem Photobiol* **73**, 630 (2001).

7. J. W. Lee, I. Lee, E. Greenbaum, Imaging Nanometer Metallocatalysts Formed by Photosynthetic Deposition of Water-Soluble Transition-Metal Compounds. *J Phys Chem B* **109**, 5409–5413 (2005).

8. J. W. Lee, C. V. Tevault, S. L. Blankinship, R. T. Collins, E. Greenbaum, Photosynthetic Water Splitting: *In situ* Photoprecipitation of Metallocatalysts for Photoevolution of Hydrogen and Oxygen. *Energy & Fuels* **8**, 770–773 (1994).

9. E. Greenbaum, Interfacial photoreactions at the photosynthetic membrane interface: an upper limit for the number of platinum atoms required to form a hydrogen-evolving platinum metal catalyst. *J Phys Chem* **92**, 4571–4574 (1988).

10. E. Greenbaum, Platinized Chloroplasts: A Novel Photocatalytic Material. *Science (1979)* **230**, 1373–1375 (1985).

11. M. Gorka, J. Schartner, A. van der Est, M. Rögner, J. H. Golbeck, Light-Mediated Hydrogen Generation in Photosystem I: Attachment of a Naphthoquinone–Molecular Wire–Pt Nanoparticle to the A_{1A} and A_{1B} Sites. *Biochemistry* **53**, 2295–2306 (2014).

12. M. Gorka, *et al.*, Electron transfer from the A_{1A} and A_{1B} sites to a tethered Pt nanoparticle requires the FeS clusters for suppression of the recombination channel. *J Photochem Photobiol B* **152**, 325–334 (2015).

13. C. E. Lubner, D. A. Bryant, J. H. Golbeck, "Wired Reaction Centers" in *Molecular Solar Fuels*, (The Royal Society of Chemistry, 2011), pp. 464–505.

14. R. A. Grimme, C. E. Lubner, J. H. Golbeck, Maximizing H_2 production in Photosystem I/dithiol molecular wire/platinum nanoparticle bioconjugates. *Dalton Transactions* 10106 (2009).

15. K. A. Walters, J. H. Golbeck, Designing a modified clostridial 2[4Fe–4S] ferredoxin as a redox coupler to directly link photosystem I with a Pt nanoparticle. *Photosynth Res* **143**, 165–181 (2020).

16. S. C. Silver, *et al.*, Protein Delivery of a Ni Catalyst to Photosystem I for Light-Driven Hydrogen Production. *J Am Chem Soc* **135**, 13246–13249 (2013).

17. C. Greening, *et al.*, Genomic and metagenomic surveys of hydrogenase distribution indicate H_2 is a widely utilised energy source for microbial growth and survival. *ISME J* **10**, 761–777 (2016).

18. P. M. Vignais, B. Billoud, Occurrence, Classification, and Biological Function of Hydrogenases: An Overview. *Chem Rev* **107**, 4206–4272 (2007).

19. M. J. Lacasse, D. B. Zamble, [NiFe]-Hydrogenase Maturation. *Biochemistry* **55**, 1689–1701 (2016).

20. M. Degli Esposti, *et al.*, Alpha proteobacterial ancestry of the [Fe-Fe]-hydrogenases in anaerobic eukaryotes. *Biol Direct* **11**, 34 (2016).

21. B. Ghysels, D. Godaux, R. F. Matagne, P. Cardol, F. Franck, Function of the Chloroplast Hydrogenase in the Microalga Chlamydomonas: The Role of Hydrogenase and State Transitions during Photosynthetic Activation in Anaerobiosis. *PLoS One* **8**, e64161 (2013).

22. G. Torzillo, A. Scoma, C. Faraloni, L. Giannelli, Advances in the biotechnology of hydrogen production with the microalga *Chlamydomonas reinhardtii*. *Crit Rev Biotechnol* **35**, 485–496 (2015).

23. C. E. Lubner, *et al.*, Solar hydrogen-producing bionanodevice outperforms natural photosynthesis. *Proceedings of the National Academy of Sciences* **108**, 20988–20991 (2011).

24. S. Morra, M. Arizzi, F. Valetti, G. Gilardi, Oxygen Stability in the New [FeFe]-Hydrogenase from *Clostridium beijerinckii* SM10 (*Cb*A5H). *Biochemistry* **55**, 5897–5900 (2016).

25. M. Ihara, *et al.*, Light-driven Hydrogen Production by a Hybrid Complex of a [NiFe]-Hydrogenase and the Cyanobacterial Photosystem I. *Photochem Photobiol* **82**, 676–682 (2006).

26. J. Appel, V. Hueren, M. Boehm, K. Gutekunst, Cyanobacterial *in vivo* solar hydrogen production using a photosystem I–hydrogenase (PsaD-HoxYH) fusion complex. *Nat Energy* **5**, 458–467 (2020).

27. K. A. Vincent, *et al.*, Electrochemical Definitions of O_2 Sensitivity and Oxidative Inactivation in Hydrogenases. *J Am Chem Soc* **127**, 18179–18189 (2005).

28. J. C. Fontecilla-Camps, A. Volbeda, C. Cavazza, Y. Nicolet, Structure/Function Relationships of [NiFe]- and [FeFe]-Hydrogenases. *Chem Rev* **107**, 4273–4303 (2007).

29. J. W. Peters, *et al.*, [FeFe]- and [NiFe]-hydrogenase diversity, mechanism, and maturation. *Biochimica et Biophysica Acta (BBA) - Molecular Cell Research* **1853**, 1350–1369 (2015).

30. A. Kanygin, *et al.*, Rewiring photosynthesis: a photosystem I-hydrogenase chimera that makes H_2 *in vivo*. *Energy Environ Sci* **13**, 2903–2914 (2020).

31. A. Kanygin, A. Smith, V. Nagy, S. Z. Tóth, K. E. Redding, Interplay between hydrogen production and photosynthesis in a green alga expressing an active photosystem I-hydrogenase chimera. *Int J Hydrogen Energy* **47**, 21969–21983 (2022).

32. S. Morra, Fantastic [FeFe]-Hydrogenases and Where to Find Them. *Front Microbiol* **13** (2022).

33. K. D. Swanson, *et al.*, [FeFe]-Hydrogenase Oxygen Inactivation Is Initiated at the H Cluster 2Fe Subcluster. *J Am Chem Soc* **137**, 1809–1816 (2015).

34. S. T. Stripp, *et al.*, How oxygen attacks [FeFe] hydrogenases from photosynthetic organisms. *Proceedings of the National Academy of Sciences* **106**, 17331–17336 (2009).

35. A. Kubas, *et al.*, Mechanism of O_2 diffusion and reduction in FeFe hydrogenases. *Nat Chem* **9**, 88–95 (2017).

36. N. Chongdar, *et al.*, Unique Spectroscopic Properties of the H-Cluster in a Putative Sensory [FeFe] Hydrogenase. *J Am Chem Soc* **140**, 1057–1068 (2018).

37. J. Barber, Photosynthetic generation of oxygen. *Philosophical Transactions of the Royal Society B: Biological Sciences* **363**, 2665–2674 (2008).

38. P. S. Corrigan, J. L. Tirsch, A. Silakov, Investigation of the Unusual Ability of the [FeFe] Hydrogenase from *Clostridium beijerinckii* to Access an O_2-Protected State. *J Am Chem Soc* **142**, 12409–12419 (2020).

39. M. Winkler, *et al.*, A safety cap protects hydrogenase from oxygen attack. *Nat Commun* **12**, 756 (2021).

40. P. S. Corrigan, S. H. Majer, A. Silakov, Evidence of Atypical Structural Flexibility of the Active Site Surrounding of an [FeFe] Hydrogenase from *Clostridium beijerinkii*. *J Am Chem Soc* **145**, 11033–11044 (2023).

41. A. Rutz, *et al.*, Increasing the O_2 Resistance of the [FeFe]-Hydrogenase *Cb*A5H through Enhanced Protein Flexibility. *ACS Catal* **13**, 856–865 (2023).

42. Q. Xu, *et al.*, Mutational analysis of photosystem I polypeptides in *Synechocystis sp.* PCC 6803. Subunit requirements for reduction of $NADP^+$ mediated by ferredoxin and flavodoxin. *Journal of Biological Chemistry* **269**, 21512–21518 (1994).

43. G. Moal, B. Lagoutte, Photo-induced electron transfer from photosystem I to $NADP^+$: Characterization and tentative simulation of the *in vivo* environment. *Biochimica et Biophysica Acta (BBA) - Bioenergetics* **1817**, 1635–1645 (2012).

44. H. Medipally, M. Mann, C. Kötting, W. J. H. van Berkel, M. M. Nowaczyk, A Clickable Photosystem I, Ferredoxin, and Ferredoxin $NADP^+$ Reductase Fusion System for Light-Driven NADPH Regeneration. *ChemBioChem* **24** (2023).

45. C. Léger, S. Dementin, P. Bertrand, M. Rousset, B. Guigliarelli, Inhibition and Aerobic Inactivation Kinetics of *Desulfovibrio fructosovorans* NiFe Hydrogenase Studied by Protein Film Voltammetry. *J Am Chem Soc* **126**, 12162–12172 (2004).

46. C. Léger, *et al.*, Enzyme Electrokinetics: Using Protein Film Voltammetry To Investigate Redox Enzymes and Their Mechanisms. *Biochemistry* **42**, 8653–8662 (2003).

47. M. del Barrio, *et al.*, Electrochemical Investigations of Hydrogenases and Other Enzymes That Produce and Use Solar Fuels. *Acc Chem Res* **51**, 769–777 (2018).

48. Note that E_{switch} is a kinetic parameter, changing its value depending on the scan rate in CV. Thus, the comparison is only valid for data obtained at the same scan rates.

49. R. M. Evans, *et al.*, Principles of Sustained Enzymatic Hydrogen Oxidation in the Presence of Oxygen – The Crucial Influence of High Potential Fe–S Clusters in the Electron Relay of [NiFe]-Hydrogenases. *J Am Chem Soc* **135**, 2694–2707 (2013).

50. H. Makita, N. Zhao, G. Hastings, Time-resolved visible and infrared difference spectroscopy for the study of photosystem I with different quinones incorporated into the A_1 binding site. *Biochimica et Biophysica Acta (BBA) - Bioenergetics* **1847**, 343–354 (2015).

51. J. Sun, *et al.*, Evidence that histidine forms a coordination bond to the A_{0A} and A_{0B} chlorophylls and a second H-bond to the A_{1A} and A_{1B} phylloquinones in $M688H_{PsaA}$ and $M668H_{PsaB}$ variants of *Synechocystis sp.* PCC 6803. *Biochimica et Biophysica Acta (BBA) - Bioenergetics* **1837**, 1362–1375 (2014).

52. V. Kurashov, *et al.*, Critical evaluation of electron transfer kinetics in P_{700}–F_A/F_B, P_{700}–F_X, and P_{700}–A_1 Photosystem I core complexes in liquid and in trehalose glass. *Biochimica et Biophysica Acta (BBA) - Bioenergetics* **1859**, 1288–1301 (2018).

53. I. R. Vassiliev, Y. S. Jung, M. D. Mamedov, Semenov AYu, J. H. Golbeck, Near-IR absorbance changes and electrogenic reactions in the microsecond-to-second time domain in Photosystem I. *Biophys J* **72**, 301–315 (1997).

54. S. W. Provencher, CONTIN: A general purpose constrained regularization program for inverting noisy linear algebraic and integral equations. *Comput Phys Commun* **27**, 229–242 (1982).

55. L. Yu, J. Zhao, U. Muhlenhoff, D. A. Bryant, J. H. Golbeck, PsaE Is Required for *in Vivo* Cyclic Electron Flow around Photosystem I in the Cyanobacterium *Synechococcus sp.* PCC 7002. *Plant Physiol* **103**, 171–180 (1993).

56. M. Ihara, H. Nakamoto, T. Kamachi, I. Okura, M. Maeda, Photoinduced Hydrogen Production by Direct Electron Transfer from Photosystem I Cross-Linked with Cytochrome c_3 to [NiFe]-Hydrogenase. *Photochem Photobiol* **82**, 1677–1685 (2006).

57. C. E. Lubner, *et al.*, Wiring an [FeFe]-Hydrogenase with Photosystem I for Light-Induced Hydrogen Production. *Biochemistry* **49**, 10264–10266 (2010).

58. M. Gorka, J. H. Golbeck, Generating dihydrogen by tethering an [FeFe]hydrogenase via a molecular wire to the A_{1A}/A_{1B} sites of photosystem I. *Photosynth Res* **143**, 155–163 (2020).

59. L. M. Utschig, S. C. Silver, K. L. Mulfort, D. M. Tiede, Nature-Driven Photochemistry for Catalytic Solar Hydrogen Production: A Photosystem I–Transition Metal Catalyst Hybrid. *J Am Chem Soc* **133**, 16334–16337 (2011).

60. L. M. Utschig, *et al.*, Photocatalytic Hydrogen Production from Noncovalent Biohybrid Photosystem I/Pt Nanoparticle Complexes. *J Phys Chem Lett* **2**, 236–241 (2011).

61. C. E. Lubner, R. Grimme, D. A. Bryant, J. H. Golbeck, Wiring Photosystem I for Direct Solar Hydrogen Production. *Biochemistry* **49**, 404–414 (2010).

62. R. A. Grimme, C. E. Lubner, D. A. Bryant, J. H. Golbeck, Photosystem I/Molecular Wire/Metal Nanoparticle Bioconjugates for the Photocatalytic Production of H_2. *J Am Chem Soc* **130**, 6308–6309 (2008).

63. A. M. Applegate, C. E. Lubner, P. Knörzer, T. Happe, J. H. Golbeck, Quantum yield measurements of light-induced H_2 generation in a photosystem I–[FeFe]-H_2ase nanoconstruct. *Photosynth Res* **127**, 5–11 (2016).

64. K. K. Niyogi, Photoprotection Revisited: *Genetic and Molecular Approaches*. *Annu Rev Plant Physiol Plant Mol Biol* **50**, 333–359 (1999).

65. M. A. Kozuleva, B. N. Ivanov, The Mechanisms of Oxygen Reduction in the Terminal Reducing Segment of the Chloroplast Photosynthetic Electron Transport Chain. *Plant Cell Physiol* pcw035 (2016). https://doi.org/10.1093/pcp/pcw035.

66. M. A. Kozuleva, A. A. Petrova, M. D. Mamedov, A. Yu. Semenov, B. N. Ivanov, O_2 reduction by photosystem I involves phylloquinone under steady-state illumination. *FEBS Lett* **588**, 4364–4368 (2014).

67. I. R. Vassiliev, Y.-S. Jung, F. Yang, J. H. Golbeck, PsaC Subunit of Photosystem I Is Oriented with Iron-Sulfur Cluster F_B as the Immediate Electron Donor to Ferredoxin and Flavodoxin. *Biophys J* **74**, 2029–2035 (1998).

68. M. K. Akhtar, P. R. Jones, Deletion of iscR stimulates recombinant clostridial Fe–Fe hydrogenase activity and H_2-accumulation in *Escherichia coli* BL21(DE3). *Appl Microbiol Biotechnol* **78**, 853–862 (2008).

69. R. Jeanjean, A. Latifi, H. C. P. Matthijs, M. Havaux, The PsaE subunit of photosystem I prevents light-induced formation of reduced oxygen species in the cyanobacterium *Synechocystis sp.* PCC 6803. *Biochimica et Biophysica Acta (BBA) - Bioenergetics* **1777**, 308–316 (2008).

FIGURES AND TABLES

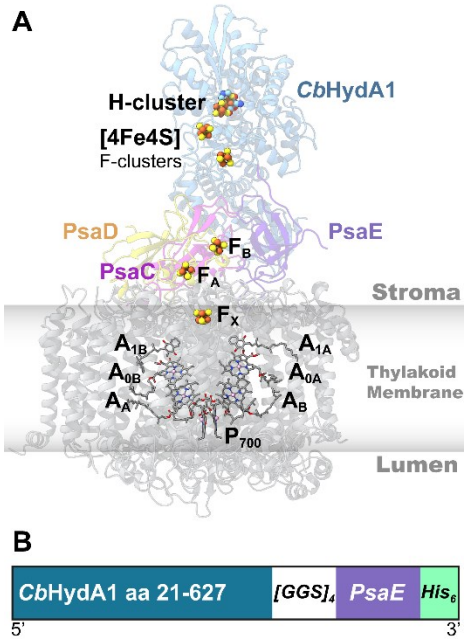

Figure 1. (A) electron-transfer cofactors of the *Cb*HydA1-PsaE:PS $I_{\Delta PsaE}$ nanoconstruct based on the structures of the PS I from *Synechococcus elongatus* (PDB: 1JB0) and [FeFe] hydrogenase from *Clostridium beijerinckii* (PDB: 6TTL). (B) Schematic representation of the protein fusion strategy employed.

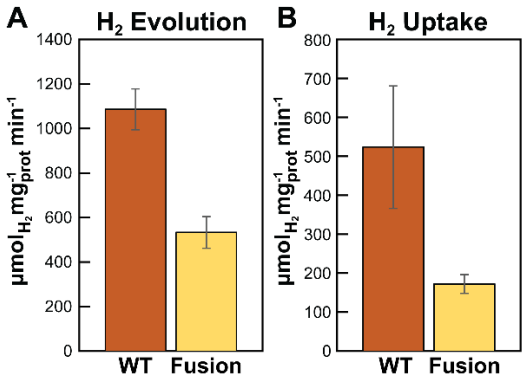

Figure 2. Specific activities for (A) H_2 evolution at pH 6.9, and (B) H_2 uptake at pH 8.0 for *Cb*HydA1$_{WT}$ (orange) and *Cb*HydA1-PsaE fusion (yellow)

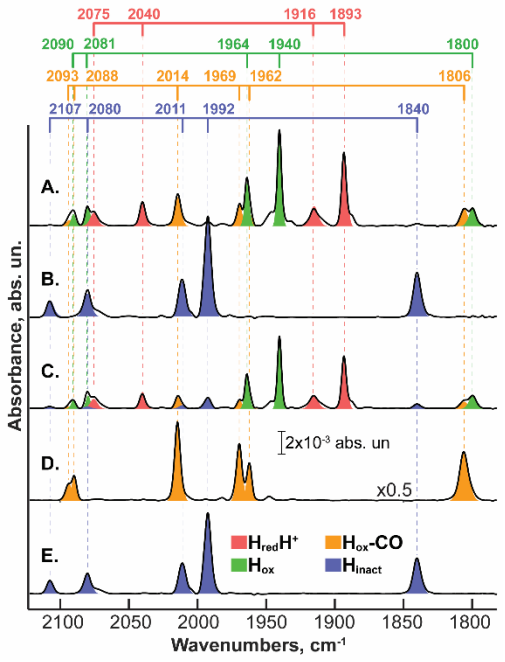

Figure 3. FTIR spectra of the *Cb*HydA1-PsaE fusion protein under various conditions: (A) As prepared, (B) After exposure to air for 20 minutes, (C) After exposure to air for 20 minutes followed by anaerobic reactivation with H_2, (D) After incubation with CO gas for 15 minutes, and (E) After incubation with CO gas for 15 minutes followed by exposure to air for 20 minutes. The shaded areas designate specific states of the H-cluster with color-coding indicated above trace (E). The y-scale is shown as a bar below trace C. Trace D was scaled by 0.5.

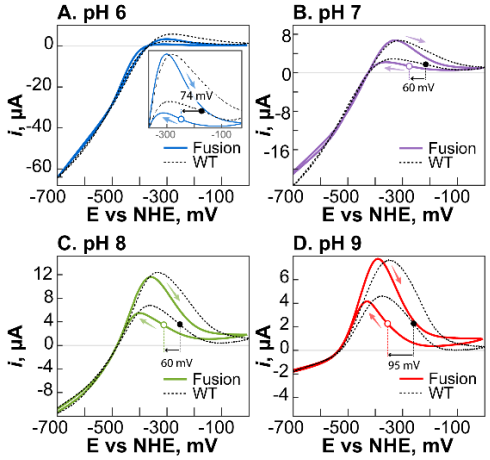

Figure 4. Room temperature cyclic voltammetry measurements of *Cb*HydA1-PsaE fusion protein adsorbed on a rotating disc graphite electrode measured at pH 6.0 (A), pH 7.0 (B), pH 8.0 (C) and pH 9.0 (D). Black dashed lines represent data for *Cb*HydA1$_{WT}$ obtained under similar conditions. Experimental conditions: scan rate, 10 mV/s; working electrode rotated at 1000 rpm; atmosphere, 1 atm of H_2.

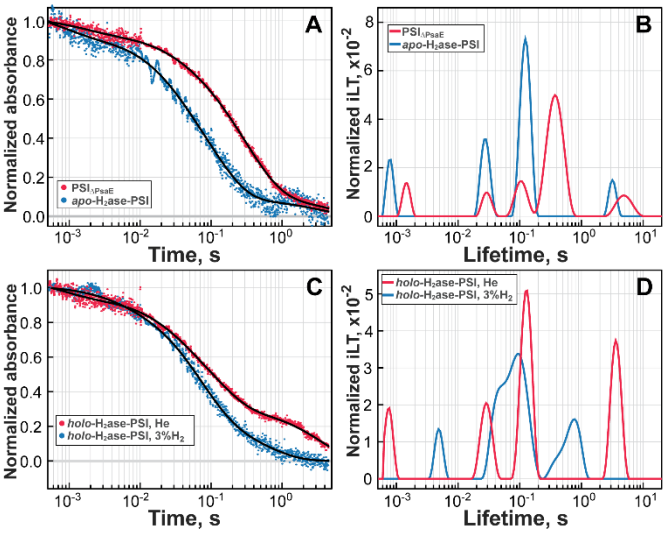

Figure 5. Anaerobic $P_{700}^{\bullet+}$ reduction kinetics after a 532 nm actinic flash. (A) PS $I_{\Delta PsaE}$ (red) PS $I_{\Delta PsaE}$:apo-*Cb*HydA1-PsaE (blue) ; (B) CONTIN inverse Laplace transformation (iLT) of A. (C) PS $I_{\Delta PsaE}$:holo-*Cb*HydA1-PsaE under 3%H, 97% N_2 (blue) and under 100% He (red). (D) CONTIN iLT of C. $P_{700}^{\bullet+}$ was monitored by absorbance at 830 nm. Traces in (B) and (D) are normalized to the sum of preexponential factors. Black traces in (A) and (C) are reconstructions of kinetics using (B) and (D) respectively.

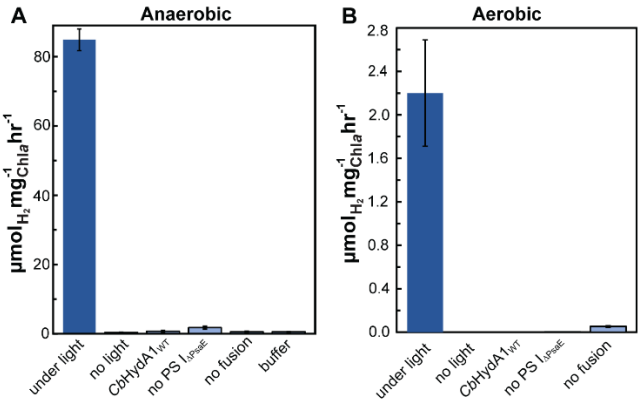

Figure 6. Light-induced H_2 generation rates for the *Cb*HydA1-PsaE:PS $I_{\Delta PsaE}$ nanoconstruct under (A) anaerobic and (B) aerobic conditions (dark blue), along with controls for each condition (light blue).